

THE ARECIBO DUAL-BEAM SURVEY: THE H I MASS FUNCTION OF GALAXIES

JESSICA L. ROSENBERG¹ & STEPHEN E. SCHNEIDER

Department of Astronomy, University of Massachusetts, Amherst, MA 01003

jrosenbe@casa.colorado.edu

schneider@messier.astro.umass.edu

Draft version October 5, 2018

ABSTRACT

We use the H I-selected galaxy sample from the Arecibo Dual-Beam Survey (Rosenberg & Schneider 2000) to determine the shape of the H I mass function of galaxies in the local universe using both the step-wise maximum likelihood and the $1/\mathcal{V}_{tot}$ methods. Our survey region spanned all 24 hours of right ascension at selected declinations between 8° and 29° covering $\sim 430 \text{ deg}^2$ of sky in the main beam. The survey is not as deep as some previous Arecibo surveys, but it has a larger total search volume and samples a much larger area of the sky. We conducted extensive tests on all aspects of the galaxy detection process, allowing us to empirically correct for our sensitivity limits, unlike the previous surveys. The mass function for the entire sample is quite steep, with a power-law slope of $\alpha \approx -1.5$. We find indications that the slope of the H I mass function is flatter near the Virgo cluster, suggesting that evolutionary effects in high density environments may alter the shape of the H I mass function. These evolutionary effects may help to explain differences in the H I mass function derived by different groups. We are sensitive to the most massive sources ($\log M > 5 \times 10^{10} M_\odot$) over most of the declination range, $\sim 1 \text{ sr}$, and do not detect any massive low surface brightness galaxies. These statistics restrict the population of Malin 1-like galaxies to $< 5.5 \times 10^{-6} \text{ Mpc}^{-3}$.

Subject headings: galaxies: mass function — radio lines: galaxies

1. INTRODUCTION

One of the main motivations for the Arecibo Dual-Beam Survey (ADBS, Rosenberg & Schneider 2000, hereafter Paper 1) was to determine the shape of the H I mass function and, in particular, to determine the amount of mass tied up in low H I-mass galaxies. Our data indicate that the H I mass function is quite steep down to our effective sensitivity limit of about $3 \times 10^7 M_\odot$. As parameterized by a Schechter function, we find a power law slope of $\alpha = -1.5$.

The faint end slope of the H I mass function has been the focus of considerable controversy, resulting in uncertainty about the fraction of the overall hydrogen budget contributed by low-mass galaxies. We suggest that the differences found between different groups are at least partially caused by environmental influences, with ram-pressure stripping and merging in high-density environments resulting in the depletion of low mass H I sources.

Most of the shallower slopes ($\alpha \approx -1.2$) for the H I mass function have been derived from optically-selected samples in the field (Huchtmeier 2000, Briggs & Rao 1993), or in clusters (Briggs & Rao 1993) or H I-selected samples in high density regions like the Canes Venatici group (Kraan-Korteweg et al. 1999), Centaurus A (Banks et al. 1999), or Ursa Major (Verheijen 2000). The results for the faint end slope in the field have been more varied. Some H I-selected samples (Zwaan et al. 1997) have also suggested a slope of $\alpha \approx -1.2$, while other studies indicate that the slope might be steeper. Early Parkes survey results suggest a slope of $\alpha \approx -1.5$ (Henning et al. 2000; Kilborn et al. 2001), and our analysis of two earlier Arecibo surveys (Schneider, Spitzak, & Rosenberg 1998, hereafter SSR) suggested

a steep faint-end rise similar to that of some optical field galaxy samples (Loveday 1997; Driver & Phillipps 1996).

In addition to the effects of environment, we believe a significant source of discrepancies between surveys arise from differences in the analysis methodology and the determination of sensitivity limits. One of the most important innovations of the ADBS is the introduction of “synthetic” sources that were carried through the entire data reduction stream in order to accurately characterize our recovery rate (Paper 1). Most previous surveys have relied on blanket claims of $N\text{-}\sigma$ sensitivity without demonstrating their completeness at the quoted level. In fact, most samples we have examined fail $\mathcal{V}/\mathcal{V}_{max}$ completeness tests (SSR; Schneider & Schombert 2000).

The data for this analysis are derived from the Arecibo Dual-Beam Survey (see Paper 1 for survey details). This is a “blind” H I driftscan survey that covers $\sim 430 \text{ deg}^2$ in the main beam. The final galaxy tally is 265 sources in the velocity range -654 to 7977 km s^{-1} . These 265 galaxies represent all of the sources detected in by-eye examinations of the Arecibo data that were reconfirmed at Arecibo and/or the VLA. Seven of the galaxies have $M_{HI} < 10^8 M_\odot$, almost as many low mass sources as found in all earlier blind surveys combined (we use $H_0 = 75 \text{ km s}^{-1} \text{ Mpc}^{-3}$ throughout). The average *rms* noise of the survey spectra is 3.5 mJy so a $10^8 M_\odot$ source with a 50 km s^{-1} velocity width would be a $5\text{-}\sigma$ detection at $22 h_{75}^{-1} \text{ Mpc}$ (1650 km s^{-1}).

In §2 we describe the survey sensitivity and the relationship between a galaxy’s HI mass and its observed flux as a function of position, frequency, and distance. In §3 we

¹ Present address: Center for Astrophysics & Space Sciences, Department of Astrophysical and Planetary Sciences, University of Colorado, Boulder, CO 80309

describe the probability of detecting a galaxy as a function of the profile linewidth and the observed flux. This section makes use of the “synthetic” sources inserted in the data to determine these probabilities. In §4 we derive the field mass function for the ADBS using two standard techniques: the stepwise maximum likelihood (SWML) and the $1/\mathcal{V}_{tot}$ methods. We also examine whether the mass function might be significantly altered by different assumptions like varying our minimum velocity cutoff, our distance determination method, or the shape of the completeness function. In §5 we discuss the influence of galaxy density on the shape of the H I mass function, and show how the mass function might be affected by making corrections for large scale structure (in the $1/\mathcal{V}_{tot}$ method). In §6 we examine the limits that the survey places on the population of galaxies with extremely high H I masses, and in §7 we summarize our results.

2. SURVEY SENSITIVITY

The interpretation of H I surveys requires accounting for variations in sensitivity as a function of source position and redshift. In addition, all current blind H I surveys are only sensitive to low mass sources at low redshifts, which can potentially introduce large errors in nearby source distances. Optical surveys have similar issues—caused by vignetting, K-corrections, and magnitude limits—but these are generally much less important.

Whenever possible, we have established empirical relationships to describe our survey’s sensitivity and/or applied alternate methods to test the robustness of our results. In the following sections we describe the noise levels for our spectra throughout the survey (§2.1), and then study the relationship between a galaxy’s HI mass and its observed flux as a function of position (§2.2), frequency (§2.3), and distance (§2.4).

2.1. Baseline Noise and Coverage

The average *rms* sensitivity for individual spectra, after Hanning smoothing to a resolution of 32 km s^{-1} , was $\sigma_1 = 3.5 \text{ mJy}$. The variation around this value was small except for occasional episodes of heavy broadband interference which occurred in about 2% of our observations. Since none of our 265 sources were detected during these high-noise episodes, we have eliminated them from further consideration.

Over 31% of the area observed, the ADBS scanned the position only once, the remainder was covered at least twice. We did not coadd spectra where they overlapped because there were occasionally slight differences in the data-taking rate, brief gaps associated with data dumps, and episodes of broadband interference. All of these small differences would have left us with a data cube with very complex noise variations if we had coadded the data. Rather, we examined doubly-covered regions in parallel, using the duplication of faint sources to help us more reliably identify sources.

Even though the spectra in double-covered regions were not coadded, examining the data in parallel allowed us to detect fainter sources. This sensitivity improvement is reflected by our detecting 77% of our sources in the 69% of the survey area that was double-covered. We estimated the improvement in sensitivity by comparing $\mathcal{V}/\mathcal{V}_{max}$ com-

pleteness tests (see SSR) for single- and double-covered regions. We find that double coverage was equivalent to a noise reduction by a factor of 1.2, giving an effective *rms* noise for double-covered regions of $\sigma_2 = 2.9 \text{ mJy}$.

2.2. Position Dependence

Because the ADBS was a driftscan survey, the sensitivity to sources decreased with increasing declination-offset, $\Delta\delta$, from each feed’s fixed declination. The theoretical “integrated” beam of the survey, which describes the sensitivity decrease, is shown in Paper 1. The actual sensitivity is more complicated since it depends on the convolution of each galaxy’s H I distribution with a beam that is not precisely azimuthally symmetric and which is sampled at intervals that do not integrate each galaxy’s entire flux, $\int S dv$, as it passes through the beam. We determined the galaxies’ fluxes ($\int S dv$) with follow-up, centered observations at Arecibo and the VLA, and compared these with their originally observed fluxes ($\int S_{obs} dv$) as a function of their declination offset. To simplify the notation, we will call these integrated fluxes or “signals” \mathcal{S} and \mathcal{S}_{obs} respectively. We found that the empirical relationship between the two was well fit by the function:

$$f(\Delta\delta) = \frac{\mathcal{S}}{\mathcal{S}_{obs}} \approx 1 + 0.28 \cdot \text{abs}(\Delta\delta)^{1.8} \quad (1)$$

for $\Delta\delta$ in arcmin. The first sidelobe is at $\Delta\delta \sim 4.4'$ (see Paper 1) where f drops to about 0.2. Beyond $\Delta\delta = 4.4'$ the correction factor is more uncertain, but we detected 20 sources with offsets up to $\Delta\delta = 12'$. The galaxies with large offsets were all high mass galaxies with extended H I distributions and had mean detection fluxes $\sim 10\%$ of their remeasured values. These 20 sources are not included in the H I mass function calculations.

2.3. Frequency Dependence

The two line-feed receiver systems used in the ADBS each had variable gain depending on the redshifted frequency of the H I signal. We determined the gain, $g(\nu)$, across the bandpass by examining continuum sources that fell within the survey region, and (following standard practice at the observatory) fitted the gain variations with a Gaussian function of frequency:

$$g(\nu) = 2^{-[2(\nu - \nu_{cen})/52]^2} \quad (2)$$

where ν_{cen} is the center frequency for the feed. For the 21 cm feed we determined this to be 1408.5 MHz; for the 22 cm feed, 1398.5 MHz. Both feeds had a half-power frequency response width of 52 MHz.

We determined the statistics for single and double sky coverage by the 21 and 22 cm feeds separately because of the differences in the feed responses. The 22 cm feed was more often affected by the occasional broadband interference and had a lower gain at the small redshifts so it was less sensitive to the lowest-mass sources, which can only be detected nearby.

2.4. Distance Estimates

The ADBS search volume includes the Virgo Cluster. This not only introduces possible problems with respect to variations in the shape of the mass function because of the environment, but also causes large uncertainties in

the redshift/distance relationship. We adopt the Tonry et al. (2000) flow model to derive distances from our measured redshifts, and assumed a Hubble constant of $H_0 = 75 \text{ km s}^{-1} \text{ Mpc}^{-1}$. We tested the sensitivity of our results to the choice of flow model by also carrying out the calculations using a simple distance estimate based on V_0 , the heliocentric velocity corrected by $300 \cos(b) \sin(l)$ for Local Group motion (de Vaucouleurs et al. 1977; also see §4.3).

The flow correction model reduces distance uncertainties, but within 6° of the center of the cluster large uncertainties are impossible to avoid so we handle this region separately in our analysis (§5.2). We believe that the Tonry model provides as effective a distance correction as is available, but it is important to note that all current blind H I surveys suffer from detecting low mass sources at small redshifts where the distance uncertainties are large. It will take a much deeper survey covering a large volume to improve this situation.

Given the distance of each source we can compute its mass in solar masses from:

$$M_{HI} = 2.36 \times 10^5 D^2 \mathcal{S}, \quad (3)$$

(Roberts 1975) where D is the distance in Mpc. Equivalently, we can predict the expected noise-free detection signal strength from a source located at any position in our survey volume as:

$$\mathcal{S}_{det} = 4.24 \times 10^{-6} \frac{g(\nu) M_{HI}}{f(\Delta\delta) D^2}. \quad (4)$$

Note that since we have an implicit relationship between D and ν , the detection signal strength can be predicted from the source mass, distance, and declination offset.

The distinction we make between \mathcal{S}_{obs} and \mathcal{S}_{det} is that the former includes noise and may suffer from peculiarities due to the specific observational conditions, like asymmetries in the beam shape. There are several other small effects that we have ignored:

(1) Variations with declination: the sky moves through the telescope beam by up to 5% faster or slower at the southernmost and northernmost of our declination strips. This actually has an even smaller percentage effect on the maximum observed signal strength because the galaxies dwell within the beam for several sampling intervals.

(2) Variations with zenith angle: Because of the Arecibo telescope’s design, there are variations with angle from the zenith. Since all of our observations were made within 11° of the zenith where there was very little “spillover,” these variations are less than a few percent.

(3) Variations with source size: If a source is larger than the beam size, the measured signal will be smaller than we predict. This proves to be unimportant for our results, because all sources that “fill the beam” have strong signals. The few sources for which there is a more accurate flux in the literature have had those values substituted (see Paper 1). This is effectively a statement that there are no galaxies with such low H I surface densities that long integrations would be required to detect them, which was shown by the deeper survey of Zwaan et al. (1997). Note that this is not necessarily the case for synthesis observations where the beam size is much smaller, and the H I surface brightness sensitivity generally poorer.

The adjustments we have applied are just for the effects that result in at least tens of percent change.

3. SENSITIVITY AND COMPLETENESS

The preceding section described how the signal strength and noise levels vary with location in the survey search volume. We turn next to the probability of detecting an H I signal of a particular linewidth w and integrated flux \mathcal{S}_{det} in a spectrum with an rms noise σ .

Previous surveys have generally attempted to make plausible assumptions about some signal level to which they believe they should be complete, but we have found (SSR; Schneider & Schombert 1999) that such claims do not pass muster with completeness tests. Since all H I surveys to date have relied to varying degrees on human-eye inspection of data, we believe it is essential to build into the detection step a means of assessing the survey completeness, \mathcal{C} , empirically.

Our approach to determining the ADBS completeness was to insert a large number of “synthetic” sources throughout the survey data (see Paper 1). The synthetic profiles were modeled to look very similar to observed H I profiles, and were inserted early in the data-processing procedure so that they would be treated like real sources, suffering, for example, the effects of automated baselining procedures. The synthetic sources were given randomized positions, line widths, and line strengths, and their locations within the data stream were unknown to us during the detection steps. By determining the rate at which we recover synthetic sources of a particular line width and signal strength, we can empirically establish the probability of detecting sources with different linewidths and signal strengths.

We find that the shape of the completeness function is basically the same for different line widths w , up to some factor in the signal strength \mathcal{S}_{det} . We can write:

$$\mathcal{C}(w, \mathcal{S}_{det}, \sigma) = C \left(\frac{\mathcal{S}_{det}}{\mathcal{N}_{eff}(w)} \right) \quad (5)$$

where $\mathcal{N}_{eff}(w)$ is an effective noise level determined empirically for different line widths. Note that synthetic sources require no corrections for declination offset or gain corrections so that we know the input, noise-free value of the detection flux. In §3.1 we explain the derivation of the line width dependence and in §3.2 the variations of completeness with signal strength.

3.1. Line Width Dependence

H I surveys have sensitivity variations depending on the velocity width of the spectral line. The same total signal \mathcal{S} spread over a larger frequency width, has a lower mean flux density and is harder to detect.²

The empirical line-width dependence is slightly different than would be predicted from basic statistical arguments, but these differences do not have a strong effect on the final determination of the mass function as we show in later sections. A statistical model of the noise dependence on line width $\mathcal{N}(w)$ is that it grows as the root sum square of the uncorrelated noise σ in individual channels. In this

² Note that there are related problems for optical surveys that behave in the opposite direction—face-on disk galaxies have a lower surface brightness and are therefore harder to detect than more edge-on disks, whereas their H I line width is narrower, so they are easier to detect.

theoretical case, the noise should grow as $w^{0.5}$. However, in our analysis of earlier Arecibo surveys (SSR), we found that the detectability of wide-line sources showed a more-rapid decline with line width than this noise model predicts. Such a behavior can be explained as an effect of baselining and other data-processing procedures that may affect wider line width signals more adversely than narrow ones.

Based on our empirical results for the synthetic sources, the signal strength at which the completeness drops to 50% increases as $w^{0.75}$, or equivalently we can describe the effective noise $\mathcal{N}_{eff} \propto \mathcal{N}w^{0.25}$. We arbitrarily set the effective noise value to match the statistical value at a linewidth of 300 km s^{-1} , yielding:

$$\mathcal{N}_{eff} = \frac{32\sigma(w_{20}/32)^{0.75}}{(300/32)^{0.25}} \quad (6)$$

where σ is the *rms* noise in Jy, w_{20} is the line width of the detected signal in km s^{-1} measured at 20% of the peak flux density, and 32 refers to our velocity resolution in km s^{-1} . Note that the choice of 300 km s^{-1} for normalizing \mathcal{N}_{eff} does not in any way affect our results since the determination of the completeness \mathcal{C} simply uses this to scale the fluxes for different linewidths.

This dependence on line width is in agreement with what we found for the surveys of Spitzak & Schneider (1998) and Zwaan et al. (1997) based on their $\mathcal{V}/\mathcal{V}_{max}$ statistics for different line widths (SSR). This suggests that the reduced sensitivity to wide-line sources may be a fairly generic property of H I surveys.

The effect of the line width dependence is that sources of the same mass are not necessarily detectable to the same distances. Therefore, in order to characterize the H I mass function, we need to detect a sufficiently large number of sources so that we have a representative sample of the different characteristics of galaxies in each mass range.

3.2. The Completeness Function

We determined the probability of detecting sources—the completeness \mathcal{C} —by the rate at which we recovered the synthetic sources as function of their signal strengths. We initially examined different line width ranges separately, but the shapes of the curves were similar, so we folded the data together, scaled by the effective noise, to empirically estimate $\mathcal{C}(\mathcal{S}_{det}/\mathcal{N}_{eff})$. Again note that we are studying the synthetic sources so we know the input, noise-free value of the detection flux. The resulting completeness function is shown in Figure 1.

The figure shows that the edge between detectability and non-detectability is not sharp. This is a combination of at least two effects: (1) noise added to sources near the limit of detectability of the survey may push sources above or below the detection threshold; and (2) the interaction of a particular line shape with the detection methods, whether automated or conducted by-eye, will introduce some uncertainty in detections near the nominal “limit.” The dashed line in the figure is an error function fit to the data. An error function is the expected result when Gaussian noise falls on top of an underlying signal.

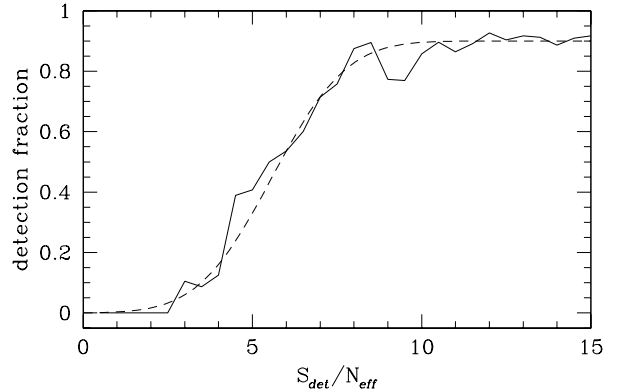


FIG. 1.— The relationship between completeness and $\mathcal{S}_{det}/\mathcal{N}_{eff}$. This function was determined using the “synthetic” sources from Paper 1. The dashed line is an error function fit to the data.

We found that the detection fraction never reached 1.0, mostly because we would occasionally lose bright sources near interference spikes or when the automated baselining procedure did not work well (see Paper 1). We found that we could not isolate this effect to a few individual frequencies, so we leave it as an overall correction that will make our estimated source densities about 10% higher.

Because of the characteristics of gaussian noise, any cutoff in signal-to-noise inevitably includes some sources below the cutoff limit and excludes some sources above it. One can approximate a step-function sensitivity by detecting sources to a deep limit and then using high sensitivity follow-up observations to eliminate all sources below where the roll-off in completeness becomes significant. Unfortunately, this would necessitate using a very high cutoff level ($\mathcal{S}/\mathcal{N} \approx 10$), and ignoring a large amount of data.

Another approach might be to choose a lower cutoff, like 5- or 7- σ , and ignore all sources that prove to be weaker than this limit upon follow-up observations. This approach will exclude less data than a high-sigma cutoff, but it has the disadvantage of uncertain effects due to the incompleteness of low-flux sources.

With knowledge of the completeness function, it is possible to retain all detected sources when estimating the mass function. We know the fraction of sources detected at any signal-to-noise level, so we can correct our estimates of the volume of space searched. Essentially, where a source’s signal strength is so weak that our probability of detection is half, we have effectively searched half as much volume at that distance.

3.3. Completeness and $\mathcal{V}/\mathcal{V}_{max}$

The $\mathcal{V}/\mathcal{V}_{max}$ test (Schmidt 1968) is often used to determine whether a survey’s sensitivity has been properly defined. The $\mathcal{V}/\mathcal{V}_{max}$ test assumes a step-function sensitivity cutoff and uniformly distributed sources. Given these conditions, the average of the volumes interior to all sources should equal half of the maximum volume within which these sources could have been detected: $\overline{\mathcal{V}/\mathcal{V}_{max}} = 0.5$.

If we allow for a roll-off in completeness, some sources will be detected that are actually weaker than whatever nominal sensitivity limit is chosen, and they will have $\mathcal{V}/\mathcal{V}_{max} > 1$. It is no longer clear what value of $\overline{\mathcal{V}/\mathcal{V}_{max}}$ should result from such a sample, or whether the test is

applicable.

Actually, it is straightforward to calculate the expected mean value of $\mathcal{V}/\mathcal{V}_{max}$ given the completeness function. We carried out a simple Monte-Carlo calculation for 10,000 uniformly-distributed sources, randomly selected according to the value of the completeness function for their predicted fluxes at their assigned distances. Defining \mathcal{V}_{max} in terms of the limiting distance for a source with a flux at the 50% completeness level, we expect $\overline{\mathcal{V}/\mathcal{V}_{max}} = 0.61$.

The detected ADBS sources have $\overline{\mathcal{V}/\mathcal{V}_{max}} = 0.60$ when measured in the same way, which is in excellent agreement with the expected value. This agreement shows that the real detected sources behave in much the same way as predicted by our completeness function, which was based purely on the synthetic sources.

4. THE H I MASS FUNCTION

4.1. Two Methods for Determining the Mass Function

Given our results for the variation of signal strength within our search volume, and the probability of detecting sources of a particular signal strength and linewidth, determining the H I mass function is, in principle, a straightforward matter. We estimate the mass function using two well-known techniques: the “ $1/\mathcal{V}_{tot}$ ” method (see SSR) and the step-wise maximum likelihood (SWML, Efstathiou et al. 1988) method.

These two techniques are complementary in several respects:

(1) The SWML method is formulated to be independent of large scale structure effects. However, the SWML method assumes that the shape of the mass function is the same everywhere, which is particularly questionable for H I because of gas-stripping and merging in high density regions. The $1/\mathcal{V}_{tot}$ method is simpler in concept and makes no prior assumptions about the uniformity of the mass-function shape.

(2) With the $1/\mathcal{V}_{tot}$ method, the overall normalization of the mass function is directly determined. Special techniques are used to normalize the results from the SWML method, which are not easily adapted to the complex positional and distance dependencies in an H I survey. Note that for neither method does the normalization affect the shape.

(3) The $1/\mathcal{V}_{tot}$ method requires the detailed knowledge of survey sensitivity over the entire search volume as worked out in §2 and 3 to calculate the total volume (\mathcal{V}_{tot}) in which a source might have been detected. By contrast, the SWML method only requires that we find the maximum distance at which a source could have been detected *at its detected position*—this is simpler, since we can just scale the detected flux for distance and frequency dependencies.

(4) We have further simplified the SWML calculation relative to the $1/\mathcal{V}_{tot}$ method by assuming a sharp cutoff in sensitivity at 7 times the effective noise \mathcal{N}_{eff} predicted for a source of that linewidth. In part, this provides a test of whether our sensitivity “roll-off” might have an important effect on the shape of the mass function.

The total volume or $1/\mathcal{V}_{tot}$ method was originally proposed by Schmidt (1968). \mathcal{V}_{tot} is the total volume within which a source *could have been* detected. If we take all the detected sources within a particular mass range summing

up $\sum 1/\mathcal{V}_{tot}$ gives us a direct estimate the number density of such sources.

Because we have determined the detailed shape of the completeness function, we are able to more accurately estimate the total effective search volume by weighting each position according to the probability of detecting a source there, as discussed in §3.2. The detectable volume for a galaxy is therefore:

$$\mathcal{V}_{tot} = \sum_{\sigma=\sigma_1, \sigma_2} A(\sigma) \int_{\Delta\delta=-4.4'}^{4.4'} \int_{D=v_{min}/H_0}^{v_{max}/H_0} \mathcal{C}(w, \mathcal{S}_{det}, \sigma) D^2 dD d(\Delta\delta) \quad (7)$$

where $A(\sigma)$ is the angular extent of the survey with the rms level σ_1 or σ_2 , for either single or double coverage, and \mathcal{C} is the completeness function described in §3. The distance variable implicitly incorporates the assumed redshift–distance relationship and the gain dependencies on frequency. The integration over distance ranges from a minimum velocity v_{min} below which confusion with Galactic H I and high velocity clouds are likely to make source detection difficult to the maximum redshift covered by our spectra, 7977 km s⁻¹. Positional and frequency dependencies are carried implicitly within \mathcal{S}_{det} which varies with distance, declination offset ($\Delta\delta$), and frequency, as discussed in §2. In practice, we carry out this integration by summing over small intervals and calculating the predicted value of \mathcal{S}_{det} at each position and velocity.

The SWML method (Efstathiou et al. 1988) was designed to directly remove the effects of density variations caused by large-scale structure. It divides the mass function into a series of bins and solves for the most likely set of relative weights for the bins. The likelihood function for each source is the ratio of the weight of its own mass bin to the sum of the weights of all of the mass bins in which a source, with the same redshift and limiting flux, could have been detected. By taking this ratio of weights, density effects are divided out. The total likelihood is the product of the likelihoods for all of the sources. A set of mass-bin weights that maximizes the total likelihood is found iteratively.

By its design, the SWML method allows each source to have a different flux limit. The method is usually used in optical surveys where the limiting flux is uniform, but there is nothing in the design of the method or most implementations of it that requires this. We use a version of the method from Kochanek et al. (2001).

The likelihood function in the SWML method assumes a sharp cutoff in the sensitivity. It could probably be adapted to include the completeness function, but as noted in the introduction to this section, we use a fixed “completeness limit” for the SWML method rather than trying to modify the routine. We use only the 210 sources brighter than 7 times the effective noise \mathcal{N}_{eff} . Because the completeness is not 100% at this limit, we will tend to slightly underestimate the number of sources near the flux limit.

Because the H I source sensitivity varies over our search volume depending on a variety of parameters (§2), it is difficult to normalize the results from the SWML method. Instead, we scale the results to match the $1/\mathcal{V}_{tot}$ results for high-mass ($> 10^9 M_\odot$) sources. The high mass sources were detectable over most of the potential search volume, so the uncertainties in their density are small. Note again

that this does not affect the calculated shape of the mass function derived by the SWML method.

We show in the remainder of this section that the two methods display substantially similar H I mass functions. Since the two methods use different approaches, this provides some reassurance that there is not a fundamental error in one of our approaches. Of course, both methods make many of the same assumptions about sensitivity, and we attempt to test those assumptions in various ways in subsequent sections.

For the $1/\mathcal{V}_{tot}$ calculation of the mass function we include 233 galaxies, all of the galaxies confirmed in the Arecibo and VLA follow-up that were originally detected within $4.4'$ of the center of the main beam and that are $> 6^\circ$ from the center of Virgo. We recognize that this is a small sample of galaxies compared to optical surveys, however, we feel we have the best characterizations of HI survey sensitivity made to date, so our conclusions are as strong as the data allow.

4.2. The H I Mass Function

Figure 2 shows the H I mass function excluding the central 6° of Virgo based on the SWML method (filled circles) and $1/\mathcal{V}_{tot}$ method (open squares). The curves in the figure are Schechter (1976) functions:

$$\Phi(M) = \frac{dn}{d \log M} = \Phi_* \ln 10 (M_{HI}/M_*)^{\alpha+1} e^{-M_{HI}/M_*} \quad (8)$$

where α is the power-law slope of the faint end, M_* is the characteristic turn-over mass, and $\ln(10/e)\Phi_*$ is the density per mass decade at M_* . The minimum χ^2 fit to the SWML points gives: $\alpha = -1.53$, $\log(M_*/M_\odot) = 9.88$, and $\Phi_0 = 0.005 \text{ Mpc}^{-3}$. (As noted earlier, the Φ_0 normalization value is ultimately based on scaling the SWML result to the $1/\mathcal{V}_{tot}$ results.) The dashed line shows the mass function fit from Zwaan et al. (1997) from their Arecibo survey: $\alpha = -1.2$, $\log(M_*/M_\odot) = 9.80$, and $\Phi_0 = 0.0059 \text{ Mpc}^{-3}$ (adjusted to $H_0 = 75 \text{ km s}^{-1} \text{ Mpc}^{-1}$).

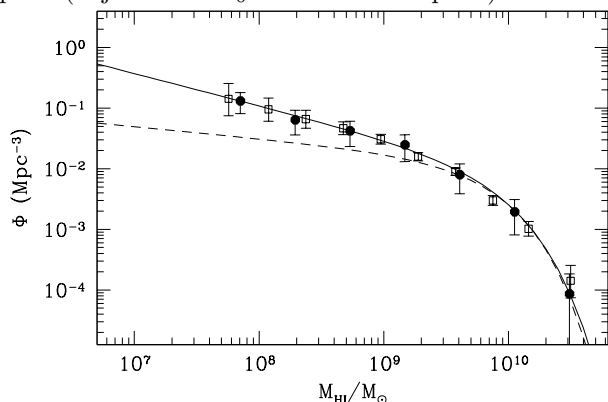


FIG. 2.— The H I mass function outside of the Virgo cluster core. The mass function is shown using both the $1/\mathcal{V}_{tot}$ method (open squares) and the step-wise maximum likelihood method (solid circles). The solid line is the best-fit Schechter function: $\alpha = -1.53$, $\log(M_*/M_\odot) = 9.88$, and $\Phi_* = 0.005 \text{ Mpc}^{-3}$. The dashed line shows the Zwaan et al (1997) Schechter model fit to the AHISS data. Error bars indicate “ $1\text{-}\sigma$ ” uncertainties; see text.

The “ $1\text{-}\sigma$ ” error bars in Fig. 2 for the $1/\mathcal{V}_{tot}$ method are based on small number statistics (Gehrels 1986). The bins

were selected by an automatic procedure that attempted to keep at least four galaxies in each bin unless the bin widths would otherwise become very small or large ($\Delta \log(M/M_\odot) > 0.4$), except at the bright end where a single galaxy was allowed to define a bin. The error bars for the SWML method include an internal estimate of the uncertainty in the normalization and are highly correlated by the nature of the method.

It is apparent from the figure that the two approaches yield very similar-shaped mass functions. It is also evident that our mass function is significantly steeper than the $\alpha = -1.2$ power law found by Zwaan et al. (1997).

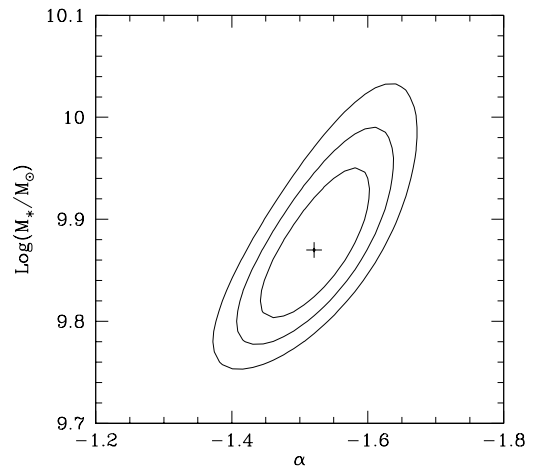


FIG. 3.— The chi-square contours of the Schechter function fit to the SWML determination of the H I mass function (shown in Figure 2). The contours represent 1, 2, and 3σ .

The shallow $\alpha = -1.2$ power law is in good agreement with our results at high masses, but it becomes successively worse at lower masses. Figure 3 shows the probable range of Schechter function parameters based on a chi-square goodness of fit to the SWML calculated mass function. Part of our difference from Zwaan et al. probably comes from our better number statistics; they had detections of only 66 sources, and only 51 with $\Delta\delta < 4.4'$. Our sample contains 7 sources with H I masses $< 10^8 M_\odot$ as compared with 2 (for $H_0 = 75 \text{ km s}^{-1}$) in Zwaan et al. (1997), 2 in Kilborn et al. (1999), and 4 in Spitzak & Schneider (1998).

We show in §4.3 that no significant changes arise when we re-examine our data set in a variety of ways. Large scale structure within our survey region also does not appear to bias our results (§4.4). However, there *are* indications of differences in the faint end slope when a survey is isolated to a cluster region (§4.5).

4.3. Effects of Analysis Procedures

There are many small choices in determining the H I mass function that might affect our results. We find, however, that our result is robust.

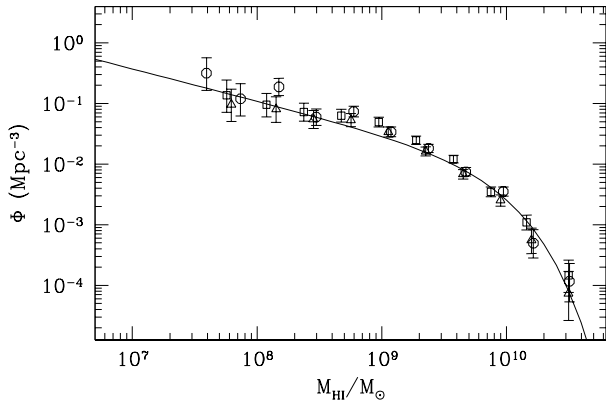


FIG. 4.— Effects on the H I mass function of varying survey parameters. The circles show the effect of using distances based on V_0 instead of the flow-corrected model of Tonry et al. (2000). The triangles show the result of narrowing the declination offset to $2'$. The squares show how the $1/\mathcal{V}_{tot}$ results change if a correction is made for the large scale structure determined from optical data in the survey region (§5.1). The Schechter function curve shows our same fit as in the previous figure to aid comparisons.

In Fig. 4, we show how the mass function is affected when we alter some of our basic assumptions. Circles in the figure show that only small changes result if we base distances on V_0 , which makes only a simple correction for Local Group motion (de Vaucouleurs et al. 1977), instead of the Tonry et al. (2000) flow model. The use of V_0 appears to make the mass function slightly steeper, but not significantly so. This suggests that distance uncertainties are unlikely to radically affect our results.

Triangles in the figure show the effect of limiting our coverage to galaxies with declination offsets smaller than $\Delta\delta < 2'$ (triangles in figure). Within these smaller offsets, our sensitivity corrections ($f(\Delta\delta)$; see §2) are less than a factor of 2.

Similarly minor changes to the H I mass function resulted when: (1) sources were detected in regions of single coverage or double coverage; (2) the minimum velocity cutoff for our volume calculations was changed from 200 km s^{-1} to 100 or 300 km s^{-1} ; or (3) sources were detected with the 21 or 22 cm feed. We note that most of the low mass sources were detected with the 21 cm feed which had better sensitivity at small redshifts. This is another difference from the Zwaan et al. (1997) data, which was based mostly on 22-cm-feed data.

4.4. Simulation Tests and the Eddington Effect

In order to test our methodology, we conducted detailed simulations of our entire procedure. We carried out these simulations to: (1) ascertain whether our completeness correction procedure had any unexpected effects; (2) address the possibility of biases that might have caused the $1/\mathcal{V}_{tot}$ to yield a different mass-function slope from an input population; and (3) determine the probable ranges for Φ in our low-mass bins where we detect a small number of sources.

Because H I surveys do not yet probe the extragalactic population very deeply, biases may be introduced due to small number statistics or from uncertainties in the distances. Besides testing our procedures, we wanted to investigate the possibility that distance uncertainties might

bias the low-mass end of our derived function. For example, Schechter (1976) discusses a bias in the shape of the luminosity function due to high mass sources at larger distances having redshifts that erroneously imply they are nearby and low-mass. Alternatively, low-mass sources may appear to have higher masses, so the overall effect on the mass function is not obvious.

Schechter showed that the “Eddington correction” for using redshift as a distance indicator can be quite large for faint objects observed at small redshifts where their distances are very uncertain. Even though we apply a flow correction model and exclude the core of Virgo from our derivation (which Schechter did not do) the residual uncertainty in distances will still most heavily influence the mass determination for low-mass sources since they are predominantly nearby.

We generated samples of galaxies that obeyed an input Schechter function, gave them H I linewidth properties that mimicked our detected galaxies, allowed for random inclinations, and located the galaxies randomly within our survey volume. Gaussian noise was added to each source and we simulated the detection steps, including effects for beam offset and frequency response, to determine which sources were detected. We also simulated all of the subsequent steps, including remeasurement of the H I flux (with appropriate levels of noise inserted), calculation of \mathcal{V}_{tot} for each source using the completeness roll-off described earlier, and finally calculated the mass function for each set of galaxies.

To explore the Eddington correction, the distances we used in our mass-function calculation were based on the sources’ redshifts, to which we added a Gaussian dispersion of 300 km s^{-1} . For sources outside the core of a cluster, this $1\text{-}\sigma$ uncertainty of 4 Mpc should represent a conservative estimate of our distance uncertainty. If the uncertainty were any larger than this we would have expected to detect some blueshifted sources outside of the Virgo core.

Each simulation required $\sim 60,000$ galaxies (down to a mass of $10^{6.5} M_\odot$), in order to “detect” ~ 233 galaxies, to match our observed sample size. We ran 1000 simulations each for an input Schechter function with a slope $\alpha = -1.53$ and for $\alpha = -1.2$, and used our same reduction programs to derive the mass function from the resulting set of detected sources.

Figure 5 shows the median source density derived for each half-decade mass interval and 1- and $2\text{-}\sigma$ (68% and 95%) confidence intervals from the 1000 simulations. The dots show the median recovered value from a population of sources assumed to follow a Schechter function with (a) $\alpha = -1.53$ and (b) $\alpha = -1.2$. The simulations show no net offset from the input mass function shape; they also provide some guidance for the size of errors that might be caused by distance uncertainties and the likelihood of detection of low mass sources below $10^{7.5} M_\odot$.

It might at first appear surprising that we find no indication of the Eddington correction. The effect does become visible when we increase the dispersion in redshifts to 600 km s^{-1} , a dispersion of 1000 km s^{-1} raised the slope of the mass function from an input value of $\alpha = -1.2$ to a derived value of about -1.4 . These are much larger distance errors than are plausible for our sample, so we conclude that the

Eddington correction is not significant for the ADBS.

The Eddington correction assumes, in effect, that more high-mass galaxies will be scattered into low mass bins than vice versa. While there is a larger volume from which to draw more massive sources that are Doppler shifted to a particular observed velocity, there is a larger space density of low-mass sources in the nearer volume. The result, at least for plausible velocity dispersions, is that comparable numbers of sources are scattered up and down into neighboring mass bins.

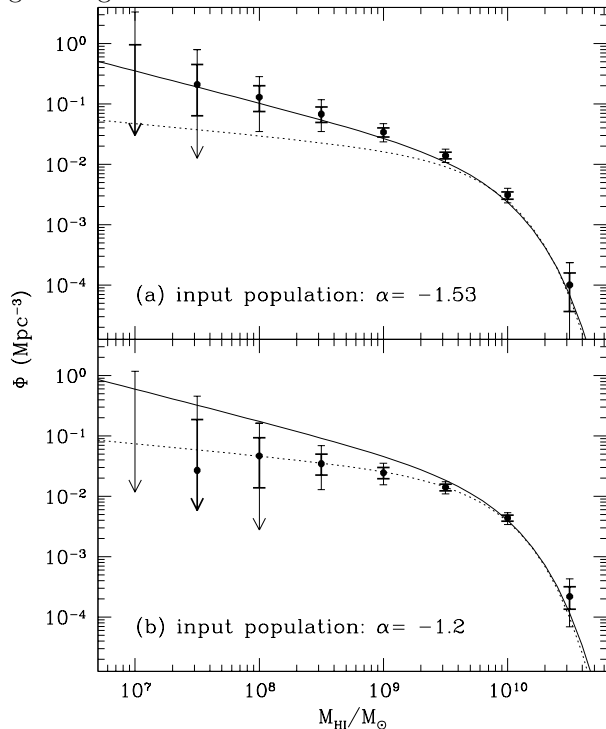


FIG. 5.— Statistical and distance-error uncertainties in the mass function. The figure shows the range of mass function results recovered from 1000 simulations of the ADBS data. The dots show the median recovered value from a population of sources assumed to follow a Schechter function with (a) $\alpha = -1.53$ or (b) $\alpha = -1.2$, shown respectively by solid and dashed curves in the figures. The simulations assumed a velocity dispersion of 300 km s^{-1} , corresponding to distance uncertainties of $\pm 4 \text{ Mpc}$. The heavy error bars show the $\pm 1\sigma$ (68.3%) range of results; the light error bars show the $\pm 2\sigma$ (95.4%) range. For the lowest mass bins, some of the expected values were zero, in which case these are marked as upper limits.

Finally, we note that in the $\alpha = -1.2$ simulation, detection of ~ 233 sources resulted in an overall density that was $\sim 1.5\times$ higher than the Zwaan et al. (1997) mass function would have predicted for our search volume. In the figure we have shifted the comparison mass functions (dashed and solid lines) upward so they pass through the simulation points. This difference is expected because our mass function results agree with Zwaan et al. at high masses, but we find a larger number of low-mass sources per unit volume than their mass function predicts. In other words, the Zwaan et al. mass function predicts that we should have detected fewer sources within our search volume than we did.

4.5. Effects of the Completeness Function on the Mass Function

For the application of the SWML method to our data, we use only sources with $\mathcal{S}_{obs}/\mathcal{N}_{eff} > 7$, and we treat them as though they would become undetectable at a distance where they would drop below this level. Thus we make no use of our completeness roll-off results, which is in keeping with the normal application of this method.

For the $1/\mathcal{V}_{tot}$ method, which has been used in all previous H I mass function studies, we consider how the results might be affected by differences in the calculation of the total detection volume for each source.

In contrast with our empirical method of determining the completeness, previous surveys have usually assumed that the effective noise depended on linewidth as $w^{0.5}$, and have claimed a step-function for the completeness behavior, often at $\mathcal{S}_{obs}/\mathcal{N} = 5$. We discuss here how such assumptions are likely to have changed the estimate of the mass function relative to our analysis.

We believe that the most critical problem with earlier surveys is *not* the details of the shape of the completeness function, but their basic assessment of where their sensitivity “cuts off.” Some surveys have used their faintest detected sources as an indication of a sensitivity limit. Figure 1 shows that using the faintest detected sources to determine this limit might imply completeness to a much lower level than was actually achieved. The total potential detection volume \mathcal{V}_{tot} predicted for each source from such a low limit will then be overestimated, and the mass function correspondingly underestimated.

The highest mass sources are bandpass limited, so exaggerating a survey’s sensitivity does not affect their predicted detection volume much.³ However, low mass sources may only be detectable to slightly beyond the minimum detection velocity, v_{min} , which is determined by such things as confusion imposed by local Galactic high velocity clouds (assumed to be 200 km s^{-1} here). If the maximum detectable distance (v_{max}/H_0) is overestimated, the predicted detection volume, $\mathcal{V}_{tot} \propto (v_{max}^3 - v_{min}^3)$ may increase more rapidly than even the cube of the distance-overestimation factor. Thus, when the sensitivity of an H I survey is exaggerated, the assumed detection volume will be overestimated more for low mass sources than high mass sources, causing the mass function to appear too shallow.

Using the roll-off in completeness introduces only a small adjustment to our estimate of the total volume in which a source could have been detected. If we substitute a step-function at the point where we reach 50% completeness, the total search volume we estimate for each source is always within $<20\%$ of the value calculated from our completeness-function-based method, and overall has a negligible effect on the mass function. Likewise, using the linewidth dependence that we have established empirically only makes a small change from assuming a $w^{0.5}$ noise dependence. In fact, if we assume a $w^{0.5}$ noise dependence, the slope of our derived mass function becomes marginally steeper.

³ The volume estimates are still somewhat affected in a driftscan survey like the ADBS or Zwaan et al. (1997) because even high-mass sources will be relatively weak at large declination offsets.

5. IS THE H I MASS FUNCTION AFFECTED BY LARGE SCALE STRUCTURE?

The question labeling this section has two aspects: (1) Does large scale structure introduce a bias into our estimate of the H I mass function? (2) Are there variations in the shape of the mass function in different density regions? In §5.1 we show that large scale structure *does not* bias our HI mass function results. In §5.2 we show that the shape of the HI mass function, on the other hand, *does* vary in different density regions.

5.1. Density Corrections

Concerns about the effect of large scale structure within our search volume should be largely eliminated by the use of the SWML method. We have noted, though, that there are potential problems with this method if the shape of the mass function varies with the local density of galaxies.

To understand possible effects of large scale structure we have used redshift data for optically cataloged galaxies to conduct a check on the amount of density variation (as a function of redshift) within our main survey region: $18.0 < \delta < 28.7^\circ$ at all right ascensions and $8.0 < \delta < 15.7^\circ$ at $0 < \alpha < 16^h$ (see Paper 1). We used galaxies with photographic magnitudes brighter than $m < 14.5$ after correcting for Galactic extinction (Schlegel et al. 1999), drawn from the NASA/IPAC Extragalactic Database (NED). We examined the NED sources in narrow redshift ranges, and found that the shape of the optical luminosity function fit a Schechter function with: $\alpha = -1.05$, $M_* = -19.9$. After correcting the velocities using the same method as for the H I measurements (Tonry et al. 2000), we derived the optical source density at each redshift by comparing the actual number counts to the predicted counts from the luminosity function. The resulting run of density with corrected velocity is shown in Fig. 6.

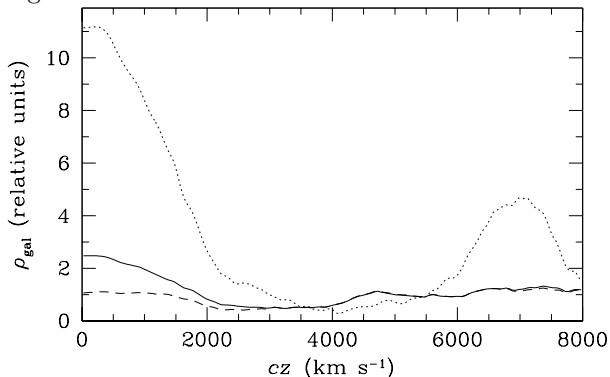


FIG. 6.— Density distribution of galaxies within the survey region based on optically selected galaxies. The solid line shows the mean density as a function of redshift for the full ADBS. The dashed line shows the density outside the core of Virgo. The dotted line shows the density within a 27° radius from the center of Virgo.

Based on the optical sample of galaxies, we find that the density within the ADBS survey region (excluding galaxies within 6° of the core of Virgo) is fairly uniform except within the interval $2000 < cz < 4000 \text{ km s}^{-1}$ where the density is about half of the other regions (solid line in figure). The higher density at other redshifts reflects (a) the local supercluster at small redshifts, (b) the Pisces-Perseus

supercluster at intermediate redshifts, and (c) the Coma cluster and associated “great wall” region at high redshifts. It is important to note that our survey region contains a mix of high and low density regions that average out to a fairly uniform density.

In the slightly underpopulated interval of $2000 < cz < 4000 \text{ km s}^{-1}$, the ADBS is primarily sensitive to galaxies with H I masses in the $8.5 < \log(M_{HI}/M_\odot) < 9.5$ range. The effect of the lower density will tend to suppress the counts in this portion of the mass function when using the $1/\mathcal{V}_{tot}$ method. We can attempt to make a density correction to the $1/\mathcal{V}_{tot}$ mass function using the optically-based density. We modified the \mathcal{V}_{tot} integral (§4.1), multiplying it by the density of sources at each velocity—essentially treating the higher density regions as having a higher detection probability (see also SSR).

The effect of this correction is shown in Fig. 4 with square symbols. Again the changes to the mass function are minor, although there is a slight elevation of source counts in estimated density of sources around $10^9 M_\odot$ as expected. After making these density corrections, the overall normalization of the mass function rises slightly to $\Phi_* = 0.0058 \text{ Mpc}^{-3}$.

Using optical estimations of the density to correct the H I-selected source counts is crude at best, but it gives us some indication of how the mass function shape and normalization might change. We expect that H I-selected sources will be less clustered than optically-selected galaxies, since galaxies in higher-density regions may be depleted of gas, so the method is likely to *over-correct* any density problems. The lack of significant changes to the $1/\mathcal{V}_{tot}$ mass function resulting from this density correction therefore indicates that the results are unlikely to be much affected by large-scale structure within the search region.

We also note that the low-H I mass galaxies in the ADBS are at similar or higher velocities than the sources in the previous Arecibo H I surveys, and the density structure we find here is more uniform than in those surveys (see SSR). Therefore our density estimate for the lowest mass bin should be less subject to bias than those earlier surveys.

5.2. Effects of Environment

The Arecibo Dual-Beam Survey covers a large swath of sky that includes the Virgo Cluster. Within the Virgo region, a significant overdensity of galaxies is evident out to about 27° from the center of the cluster (dotted line in Fig. 6). In our primary analysis we included galaxies outside of the 6° core but within 27° of the center of Virgo. Including the galaxies in the outer regions of Virgo yielded a more uniform overall density, while still avoiding the large distance ambiguities associated with the core region. This gave a mix of higher and lower density regions nearby, much as cluster and field regions also contribute to our results at higher redshifts. The region out to a radius of 27° from the center of Virgo has a mean overdensity of about a factor of 10. We examine here some possible changes in the character of the H I mass function within such a high density region.

Our sample of Virgo galaxies is small—38 galaxies within 27° of the center of the Virgo cluster, including 13 galaxies within the inner 6° . More distant clusters are not

useful for probing the H I mass function in high density regions because they are too far away for the ADBS to have detected low mass sources. We caution that small number statistics make our conclusions uncertain, but there are indications that the mass function is less steep in high density regions.

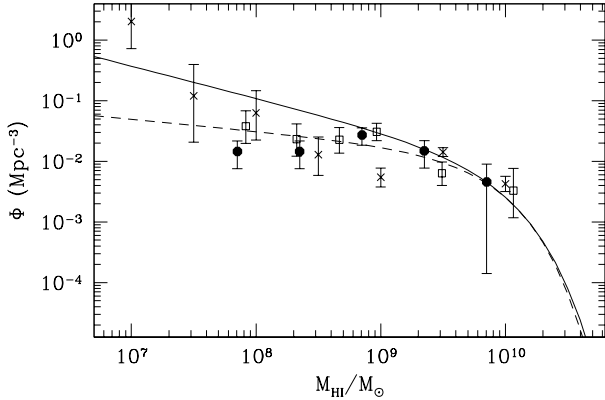


FIG. 7.— The H I mass function within the Virgo cluster region. The solid circles show the SWML estimate for galaxies within 27° of the center of the cluster and with redshifts smaller than $cz < 2300 \text{ km s}^{-1}$. The open squares show the $1/V_{tot}$ results over the same area. The solid and dashed curves are the same as in Figure 2. The data from the Arecibo Slice survey (Schneider et al. 1998) are shown as gray \times s. These data match the shallower Schechter fit where the data are being drawn from a cluster region (at the high mass end) and the steeper Schechter fit where they are being drawn from a lower density region (at the low mass end).

We calculate the mass function using the same methods as we described above. Both the SWML and $1/V_{tot}$ methods suggest a flatter mass distribution. This result was found whether we assigned all of the galaxies inside 6° with redshifts smaller than $cz < 2300 \text{ km s}^{-1}$ to a fixed distance of 16.8 Mpc or used the solution from the Tonry et al. (2000) flow model. In the figure, the SWML results use the flow model distances while the $1/V_{tot}$ results are based on a fixed distance for galaxies in the core region. We applied the density correction described in §5.1 to the $1/V_{tot}$ results. If we do not apply this correction, the normalization of our mass function would make the density higher than our earlier mass function at all masses, and about $10\times$ higher overall. Accounting for the factor of 10 overdensity in the normalization allows us to more directly compare the results.

The differences in the mass function with galaxy density may help explain the difference between our current mass function (solid line) and our earlier estimate based on the Arecibo Slice of Spitzak & Schneider (1998) which is shown by gray \times symbols in Figure 7. There is a problem with the distribution of galaxies in the Arecibo Slice (see Figure 8: all of the low mass and none of the high mass galaxies are located at low redshifts while the opposite is true at high redshifts).

The relatively limited area covered in the Arecibo Slice was dominated by the Pisces-Perseus supercluster at higher redshifts, so the mass function for H I masses greater than $\sim 10^{8.5}$ is dominated by cluster galaxies. H I masses lower than $\sim 10^{8.5}$ are drawn from lower density regions. The “turn up” that appears to occur at low masses in the Arecibo Slice is consistent with the higher mass

points being drawn from a high density region and the low mass points from a low density region. The lowest mass points are consistent with a slope of $\alpha \approx -1.5$ while the higher mass points, drawn from the higher density regions, are consistent with a slope of $\alpha = -1.2$. The joining of these two nearly independent H I mass functions produces the apparent “turn-up” in the Arecibo Slice H I mass function.

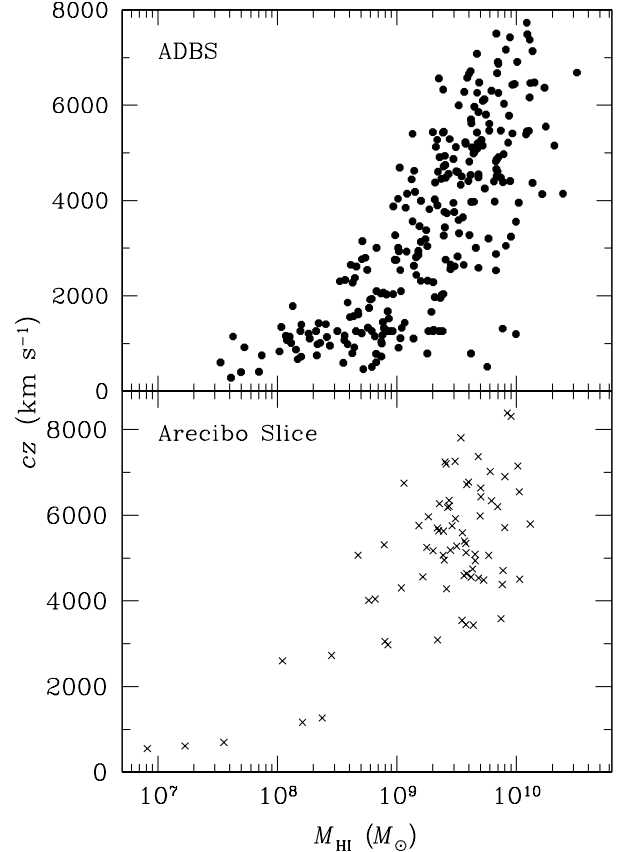


FIG. 8.— The redshifts of galaxies as a function of their H I mass in (bottom panel) the Arecibo Slice (Spitzak & Schneider 1998) and (top panel) the ADBS.

By contrast, Figure 8 demonstrates that the ADBS covered a large enough area that several high mass galaxies were detected at lower redshifts. The larger range of distances over which high mass galaxies are detected helps to anchor the relative number density of high and low mass galaxies.

6. LIMITS ON ULTRA-HIGH-MASS H I SOURCES

The galaxy Malin 1, identified by Bothun et al. (1987), has been pointed to as evidence that we might be missing a significant population of high mass, low surface brightness galaxies (Disney et al. 1987). Large, H I-rich but low surface brightness galaxies are extremely difficult to detect with standard optical techniques. H I surveys that cover large enough volumes are ideal for identifying these galaxies since they are as easy to detect as any other galaxy with a large H I mass.

The ADBS data confirm that a large population of massive H I-rich galaxies is not lurking just below the sky surface brightness limits. While our statistics at the high

mass end of the mass function are poor, we are sensitive to these galaxies in a large volume ($\sim 8 \times 10^5 \text{ Mpc}^3$) as seen by the fact that we detect high-mass sources with offsets as large as $12'$ from the center of the main beam. The mean fluxes of these galaxies are $\sim 10\%$ of their remeasured values, but with our sensitivity limits, we should be able to detect galaxies in excess of $5 \times 10^{10} M_\odot$ at these large offsets out to the limiting redshift of our survey.

With our ability to detect sources this far from the midline of the drift-scans, the declination strips nearly overlap (the strip separations alternate between 0.6° and 0.4°), which corresponds to a volume coverage of $8 \times 10^5 \text{ Mpc}^3$ over an area of $\sim 1 \text{ sr}$ for these high mass systems. Nevertheless, we detect no high mass, low surface brightness galaxies. We do not worry about column density constraints in quoting this number because even a Malin-1-like galaxy would not be resolved in most of the volume. For very nearby giants, we are only sensitive down to a column density $> 2 \times 10^{19} \text{ cm}^{-2}$.

In the nearby regime, the Zwaan et al. (1997) survey places a much tighter constraint on the population of high mass, low surface brightness galaxies because it is sensitive to column densities $> 2 \times 10^{18} \text{ cm}^{-2}$. These statistics restrict the population of Malin 1-like galaxies to $< 5.5 \times 10^{-6} \text{ Mpc}^{-3}$.

7. SUMMARY AND DISCUSSION

We have used the ADBS to study the mean H I mass over a wide range of environments, and find a steep-sloped Schechter function: $\alpha = -1.53$, $M_* = 9.88 M_\odot$, $\Phi_* = 0.0058 \text{ Mpc}^{-3}$ (the normalization is lower, $\Phi_* = 0.0048 \text{ Mpc}^{-3}$, when a density correction for large scale structure effects is not applied). The ADBS mass function results have been derived with very careful attention to the sensitivity function. We inserted “synthetic” sources which underwent all of the data processing procedures to allow us to derive the sensitivity as a function of H I line width and to derive the completeness function. Additionally, we find that our mass function results are robust to changes in an assortment of parameters such as the minimum distance and velocity flow models, and are consistent whether we use the $1/\mathcal{V}_{tot}$ or SWML method.

Our mass function differs significantly from some previous determinations, but this is probably because, in large part, previous H I mass functions were derived from optically selected samples or from samples that surveyed high density regions. It appears likely that the mass function has a different shape in clusters and in the field. There is evidence from optical surveys that the luminosity function evolves with time (Lin et al. 1999, Sawicki et al. 1997) and density may also affect the shape of the mass and luminosity functions (Phillipps et al. 1998; Wilson et al. 1997). Gas stripping, evolution, and the merger rate of galaxies, which are more significant in higher density environments, may preferentially remove gas from low mass systems or destroy them altogether. We find that the mass function in the Virgo cluster has a shallower faint-end slope, $\alpha = -1.2$, similar to that found by Verheijen et al. (2000) in the Ursa Major region, which also has an overdensity of about a factor of 10.

It is interesting to note that the changes in α we find with density may exhibit the opposite trend in optical sam-

ples. Phillipps et al. (1998) find that the slope of the luminosity function gets steeper in the higher density regions. This difference emphasizes that galaxies’ gas mass and optical luminosity are not directly related.

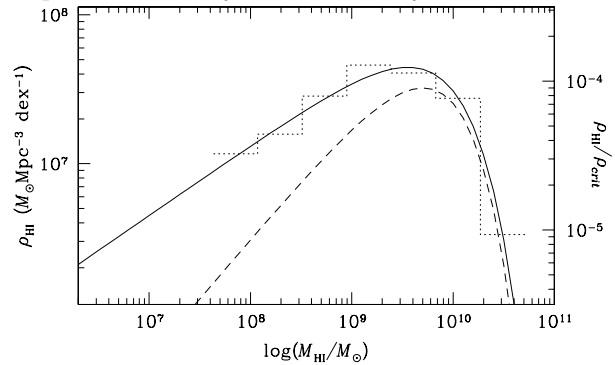


FIG. 9.— The relationship between H I mass density (left-hand y-axis) or Ω_{HI} (right-hand y-axis) and H I mass. Most of the galaxy contribution to the H I mass density and Ω_{HI} is from M_* galaxies, but the contribution from low mass sources is not negligible. The solid line fit to the histogram shows our Schechter function, $\alpha = -1.53$. The dashed line shows the Zwaan et al. (1997) value, $\alpha = -1.2$. The integral of this curve represents $\sim 1\%$ of Ω_b that resides in the H I component of galaxies.

Figure 9 shows the H I mass density of galaxies (ρ_{HI}) and the fraction of the critical density (ρ_{HI}/ρ_{crit}) contained in H I-rich galaxies as a function of the galaxy’s H I mass. This figure demonstrates that the mass contribution to (ρ_{HI}/ρ_{crit}) is largest from galaxies near M_* . However, our steep-sloped mass function indicates that the contribution from low mass sources is not negligible. The value of Ω_b inferred from D/H studies is $0.0445 h_{75}^2$ (Burles & Tytler 1998). Given this value, we find that $\sim 1\%$ ($0.000484 h_{75}^2$) of the baryonic mass is contained in the H I within galaxies. By contrast, Penton et al. (2000) have shown that $\sim 20\%$ of the baryons are tied up in low column density hydrogen, primarily H II, observed in the Lyman- α forest. The relative contribution of the high and low density material suggests that H I-rich galaxies are relatively rare concentrations of neutral gas embedded in a more substantial low density medium.

The ADBS is one of the largest surveys to date, particularly with respect to low mass sources, yet the statistics at the low mass end remain thin. Given practical limits for existing 21 cm telescopes, it seems likely that this will remain a problem for some time to come. It will therefore be vital for future surveys to carefully account for the completeness function in their design. A particularly important question for future endeavors will be the relationship between the shape of the mass function and galaxy environment. To understand evolutionary processes in galaxies, we will have to establish how the mass function changes with environment and with time.

The Digitized Sky Surveys were produced at the Space Telescope Science Institute under U.S. Government grant NAG W-2166. The images of these surveys are based on photographic data obtained using the Oschin Schmidt Telescope on Palomar Mountain and the UK Schmidt Telescope. The plates were processed into the present compressed digital form with the permission of these institu-

tions.

This research has made use of the NASA/IPAC Extragalactic Database (NED) which is operated by the Jet

Propulsion Laboratory, California Institute of Technology, under contract with the National Aeronautics and Space Administration.

REFERENCES

- Banks, G. D., Disney, M. J., Knezek, P. M., Jerjen, H., Barnes, D. G., Bhat, R., de Blok, W. J. G., Boyce, P. J., Ekers, R. D., Freeman, K. C., Gibson, B. K., Henning, P. A., Kilborn, V., Koribalski, B., Kraan-Korteweg, R. C., Malin, D. F., Minchin, R. F., Mould, J. R., Oosterloo, T., Price, R. M., Putman, M. E., Ryder, S. D., Sadler, E. M., Staveley-Smith, L., Stewart, I., Stootman, F., Vaile, R. A., Webster, R. L., & Wright, A. E. 1999, *ApJ*, 524, 612.
- Bothun, G. D., Impey, C. D., Malin, D. F., & Mould, J. R. 1987, *AJ*, 94, 23.
- Briggs, F. H. & Rao, S. 1993, *ApJ*, 417, 494.
- Burles, S. & Tytler, D. 1998, *ApJ*, 507, 732.
- de Vaucouleurs, G., Peters, W. L., & Corwin, H. G. Jr. 1977, *ApJ*, 211, 319.
- Disney, M. & Phillipps, S. 1987, *Nature*, 329, 203.
- Driver, S. P. & Phillipps, S. 1996, *ApJ*, 469, 529.
- Efstathiou, G., Ellis, R. S., & Peterson, B. A. 1988, *MNRAS*, 232, 431.
- Gehrels, N. 1986, *ApJ*, 303, 336.
- Henning, P. A., Rivers, A. J., & Staveley-Smith, L. 2000, *ASP Conference Series*, 218, 61.
- Huchtmeier, W. K., Karachentsev, I. D., & Karachentseva, V. E. 2000, *ASP Conference Series*, 218, 295.
- Kilborn, V., et al. 2001, personal communication.
- Kochanek, C. S., Pahre, M. A., Falco, E. E., Huchra, J. P., Mader, J., Jarrett, T. J., Chester, T., Cutri, R., & Schneider, S. E. 2001 *ApJ*(submitted)
- Kraan-Korteweg, R. C., van Driel, W., Briggs, F., Binggeli, B., & Mostefaoui, T. I. 1999, *A&AS*, 135, 255.
- Lin, H., Yee, H. K. C., Carlberg, R. G., Morris, S. L., Sawicki, M., Patton, D. R., Wirth, G., & Shepard, C. W. 1999, *ApJ*, 518, 533.
- Loveday, J. 1997, *ApJ*, 489, 29.
- Penton, S., Shull, J. M., & Stocke, J. T. 2000, *ApJ*, 544, 150.
- Phillipps, S., Driver, S. P., Couch, W. J., & Smith, R. M. 1998, *ApJ*, 498, 199.
- Roberts, M. S. 1975, in *Galaxies and the Universe*, eds. A. Sandage, M. Sandage, & Kristian (Chicago: Univ. Chicago Press), p. 309.
- Rosenberg, J. L. & Schneider, S. E. 2000, *ApJS*, 130, 177.
- Sawicki, M. J., Lin, H., & Yee, H. K. C. 1997, *ApJ*, 113, 15.
- Schechter, P. 1976, *ApJ*, 203, 297.
- Schlegel, D. J., Finkbeiner, D. P., & Davis, M. 1998, *apj*, 500, 525.
- Schmidt, M. 1968, *ApJ*, 151, 393.
- Schneider, S. E. & Schombert, J. 2000, *ApJ*, 530, 286.
- Schneider, S. E., Spitzak, J. G., & Rosenberg, J. L. 1998, *ApJ*, 507, 9.
- Spitzak, J. G. & Schneider, S. E. 1998, *ApJS*, 119, 159.
- Tonry, J. L., Blakeslee, J. P., Ajhar, E. A., & Dressler, A. 2000, *ApJ*, 530, 625.
- Verheijen, M. A. W., Trentham, N., Tully, R. B., & Zwaan, M. A. 2000, *ASP Conference Series*, 218, 61.
- Wilson, G., Smail, I., Ellis, R. S., & Warrick, J. C. 1997, *MNRAS*, 284, 915.
- Zwaan, M., Briggs, F. H., Sprayberry, D. & Sorar, E. 1997, *ApJ*, 490, 173.